Food & Function

Engineering cell-based microstructures to study the effect of structural complexity on in vitro bioaccessibility of a lipophilic bioactive compound

Journal:	*Food & Function*
Manuscript ID	FO-ART-02-2022-000533.R1
Article Type:	Paper
Date Submitted by the Author:	25-May-2022
Complete List of Authors:	Lu, Yixing; University of California Davis, Food Science and Technology Rai, Rewa; University of California Davis Department of Food Science and Technology, Food Science and Technology Nitin, Nitin; University of California Davis, Food Science and Technology

Engineering cell-based microstructures to study the effect of structural complexity on *in vitro* bioaccessibility of a lipophilic bioactive compound

Yixing Lu[a], Rewa Rai[a], and Nitin Nitin[ab]*

Abstract

A fundamental understanding of the influence of food microstructures on the bioaccessibility of micronutrients is vital for the design of functionally efficient foods. This study investigated the effect of microstructural features of model foods on the bioaccessibility of a bioactive compound - curcumin, using a unique bottom-up approach. In this approach, individual yeast cells with infused curcumin were coated with oppositely charged polyelectrolytes: first in poly(diallyl-dimethylammonium chloride), then in dextran sulfate or alginate, and assembled electrostatically to generate two types of cell clusters. These cell clusters were embedded in an alginate film to form a tissue-like structure. The influence of cell clustering and extracellular matrix on the release of encapsulated curcumin from cell-based microcarriers during simulated digestion was evaluated. Cell clusters that maintained their integrity during *in vitro* simulated digestion retained up to twice as much curcumin upon addition of the simulated intestinal fluid (SIF) compared to single cells during the first hour of intestinal digestion. Despite significant differences in the release profile, no spatial heterogeneity of curcumin release across a cell cluster was observed with the imaging measurements. Embedding single cells or cell clusters in calcium-crosslinked alginate films resulted in another 20-30% increase in curcumin retention and a prolonged barrier effect for more than 2 hours compared to microstructures without the films. This bottom-up approach of engineering cell-based tissue-like structures proves to be an effective method for investigating the

[a] *Department of Food Science and Technology, University of California-Davis, Davis, CA 95616, USA.*
[b] *Department of Biological and Agricultural Engineering, University of California-Davis, Davis, CA 95616, USA.*

contributions of microstructural properties of food matrices to influencing bioaccessibility of bioactives and guides future development of functional food materials.

1. Introduction

Bioaccessibility of plant-derived micronutrients has been evaluated for diverse food materials with the overall motivation to understand the factors contributing to the release profiles of various micronutrients from food matrices during digestion. Plant-derived bioactive compounds, such as curcumin, can exert different effects depending on its release site in the gut[1,2]. The chemical properties of micronutrients and microstructural properties of food matrices such as plant foods are the two major factors influencing the bioaccessibility of micronutrients. Many studies have shown that differences in the chemical nature of compounds significantly contribute to the differences in their bioaccessibility and bioavailability[3–5]. Besides, the release profiles of bioactive compounds from plant sources are significantly influenced by the microstructures of food matrices[6], generally defined as the spatial arrangement of different food elements and their mutual interactions at scales below 100 μm. In plant-based foods, the microstructural features contributing to the bioaccessibility of bioactive compounds include chemical composition of plant cells, localization of bioactives and their interaction with various cellular components[7]. However, the current approaches of studying this topic have limitations in decoupling these two effects. For instance, many studies compared the bioavailability of polyphenols from different plant origins to investigate the effect of different molecular structures and conjugation forms of the polyphenol compounds[5]. Nevertheless, such studies often ignore the impact of structural features such as the differences

in cell wall composition, localization of compounds, and the binding with food matrix elements[8].

Complementary to the influence of chemical properties of micronutrients on their bioaccessibility, some studies have evaluated the effect of food processing on the bioavailability of micronutrients. Food preparation and processing such as cutting, heating, and high-pressure treatment are known to change the microstructures of plant tissues, thus, in turn, could affect the release of micronutrients. For instance, it was reported that the release of carotenoids from plant foods occurs only after disruption of the cell walls, which may result from food processing and mastication but not during gastric digestion[9,10]. Also, cooking increased the extractability of carotenoids from food matrices by breaking down cell walls and weakening the bonding between carotenoids and pectin-like fibers in plant tissues[4]. The major limitation of using processing to study the relationship between food microstructure and nutrient bioaccessibility is that the process of modifying structural properties is not well controlled, and more than one structural feature could be impacted simultaneously by a selected processing method. Thus, changes in the compound bioaccessibility cannot be attributed to a specific structural or compositional feature. For example, grinding could break down cells and expose polyphenols to polyphenol oxidase[11] but could also increase surface area and promote accessibility of digestive enzymes, thus increasing bioaccessibility.

The current study develops a unique approach for investigating the influence of food microstructures on the bioaccessibility of micronutrients. This approach started with the infusion of a purified model bioactive compound- curcumin, in a yeast cell-based microcarrier. Subsequently, the microcarriers were assembled into cell clusters through polyelectrolytes-facilitated electrostatic interaction and then embedded in a continuous extracellular matrix to

form a tissue-like structure. Using yeast cells as micro-carriers have emerged as a practical encapsulation approach for various compounds, including curcumin[12–15]. Yeast-based carriers, based on their micro-scale size, eliminate the need to fabricate microparticles and can enhance the oxidative and thermal stability of encapsulated bioactives compared to colloidal carriers such as emulsions[16]. This study selected the vacuum-facilitated infusion process as it significantly reduces the time required for partitioning various compounds into yeast-based microcarriers[15]. The release profile of curcumin from single yeast cells during simulated digestion has been studied and reported in a previous study of ours[17]. 3D assembly of cell-based carriers into larger cell clusters was hypothesized to decrease the surface area and increase cell-cell adhesion, thus modifying the release profile of the encapsulated model bioactive compound. Additionally, the presence of an extracellular matrix adds a barrier between the cell-encapsulated bioactive compound and the digestive environment. Previous studies have shown that encapsulating curcumin in alginate matrices retarded the compound release during simulated digestion[18,19]. To the best of our knowledge, the bottom-up assembly of cells into tissue-like structures has not been utilized to understand and modulate the release of bioactive compounds during digestion processes.

The overall objective of the current study was to study the effect of cell clustering and extracellular matrix on the bioaccessibility of the encapsulated model compound during simulated gastrointestinal digestion. This approach will enhance a fundamental understanding of the role of microstructural features of cells and their assembled structures in influencing the

release of bioactives. In addition, the results of this study can enable innovations in the formulation of novel food structures to control the release of bioactive compounds.

2. Materials and methods

2.1. Materials

The following reagents used in this study: poly(diallyl dimethylammonium chloride) (PDADMAC, M_w 400,000 ~ 500,000, 20 wt.% in water), dextran sulfate sodium salt, from *Leuconostoc* spp. (DSS), alginic acid sodium salt from brown algae (ALG, medium viscosity), curcumin derived from *Curcuma longa* (Turmeric) [≥ 65%, HPLC], methanol, glycerol (≥99%), bile salts (cholic acid- deoxycholic acid sodium salt mixture), calcium chloride, and sodium phosphate, mono- and dibasic, were purchased from Sigma-Aldrich (St. Louis, MO). The enzymes used in simulated digestion fluids preparation: pepsin from porcine gastric mucosa (1064 units/mg protein), lipase from porcine pancreas Type II (100-500 units/mg protein), were also purchased from Sigma-Aldrich (St. Louis, MO). Absolute ethanol was purchased from Koptec (King of Prussia, PA) Sodium hydroxide, hydrochloric acid, and sodium chloride were purchased from Fisher Scientific (Pittsburgh, PA). Fleischmann's Active Dry yeast, *Saccharomyces cerevisiae*, was obtained from a local grocery store. Ultrapure water (18 MΩ cm) was obtained using the in-lab Milli-Q RG water ultra-purification system from EMD Millipore (Billerica, MA).

2.2. Yeast cells preparation

Native yeast cells were prepared by washing 1 g of active dry yeast twice in excess of ultrapure water. The cells were pelleted down by centrifugation at 5000 rpm for 5 minutes between each wash and once more to remove excess water.

2.3. Encapsulation of curcumin into yeast cells

Encapsulation of curcumin into yeast cells was conducted as described in a previous study[15]. Briefly, before encapsulation, 1 g of washed yeast cells were weighed into 50ml centrifuge tubes. 3.25 mL of 100 mM phosphate buffer (pH 6.5), 1.5 mL of absolute ethanol, and 250 μL of 2.5 mg/mL curcumin in absolute ethanol were added to give a 35% ethanol concentration, and 0.0625 wt.% curcumin to yeast ratio. Samples were vortexed to facilitate dispersion of yeast cells and were subjected to 99% vacuum with a hold time of 5 seconds. After vacuum infusion, the samples were centrifuged at 5000 rpm for 5 minutes, and the supernatant was decanted. The pelleted cells were then washed 4 times in 5 mL of ultrapure water, and centrifuged once more to remove excess water.

2.4. Layer-by-layer coating of yeast cells with polyelectrolytes

The method for layer-by-layer coating was adapted from previous papers reporting the coating of yeast cells using oppositely charged polyelectrolytes layers[20,21]. Polycation PDADMAC (Mw 400 ~ 500 kDa) and polyanion DSS (Mw ~5 kDa) or ALG (Mw 80~120 kDa) were deposited on native yeast cells alternately. PDADMAC (20 wt.% in water) was diluted 100 times in 0.5 wt.% NaCl aqueous solution to achieve a final PDADMAC concentration of 2 mg/mL. Yeast cells with encapsulated curcumin were suspended in PDADMAC solution at a cell density of ~10^9 cfu/mL and shaken at 200 rpm for 20 minutes. Then, the cells were separated from excess PDADMAC solution by centrifugation, and the cell pellet was washed twice with ultrapure water. Then, the resulting PDADMAC@yeast were introduced into the negatively charged polyelectrolytes: DSS or ALG (2 mg/mL in 0.5% NaCl) solution, followed by incubation at 200 rpm for 20 minutes, centrifugation, and washing (the separation and washing step for PDADMAC/DSS@yeast was modified as described in section 2.5). Three coating architectures were constructed using the layer-

by-layer deposition step: PDADMAC@yeast, PDADMAC/DSS@yeast, and PDADMAC/ALG@yeast.

2.5. Electrostatic aggregation of yeast cells

In this study, two types of cell clusters were formed by electrostatic aggregation: PDADMAC/DSS@yeast (P/D cluster), and PDADMAC@yeast+PDADMAC/ALG@yeast (P+P/A cluster). In the previous coating step, introducing PDADMAC@yeast into DSS solution, resulted in cluster formation directly. Therefore, no further aggregation step was conducted. Centrifugation of PDADMAC/DSS@yeast (P/D cluster) would lead to formation of big cell lumps that could not be easily re-dispersed by vortexing, so the cell clusters were separated from excess DSS solution by decanting supernatant after gravitational precipitation of cell clusters. The following washing step was conducted in the same way. No extensive cell flocculation was observed in the ALG coating step, therefore PDADMAC@yeast and PDADMAC/ALG@yeast were mixed at a 1 to 5 (wt. to wt.) ratio in pH 3.5, 0.5% NaCl solution for electrostatic aggregation (pH 3.5 was used to ensure stability of curcumin). After 5 minutes incubation at 200 rpm shaking, the P+P/A clusters were harvested and washed in the same way as P/D clusters.

2.6. Particle size and cell surface charge measurements

Surface charge of native yeast cells, polyelectrolytes coated cells, and cell clusters was assessed based on ζ-potential, which can be determined using electrophoretic laser scattering in a Malvern Zetasizer nano-ZS (Malvern Instruments Ltd., Malvern, Worcestershire, United Kingdom). 1 mg/mL suspension of native, coated, or clustered yeast cells was prepared in pH 3.5, 0.5 wt.% NaCl solution. ζ-potential was measured in an acidic environment because the same solution was used for electrostatic clustering of cells. 1 mL of such suspension was aliquoted to a cuvette and inserted into the measurement chamber of the Zetasizer. Particle size distribution of

native and clustered cells before and after simulated digestion were measured using a Microtrac particle size analyzer S3500 (Microtrac Inc., Montgomeryville, PA). ~600 μL of 10 mg/mL cell/cell clusters in pH 3.5, 0.5 wt.% NaCl solution was added to the sample dispersion controller filled with deionized water. Samples were mixed in the bulk water then flow through a tri-laser diffraction analyzer which measured the angular variation in intensity of light scattered as laser beams pass through a dispersed particulate sample. Particle sizes were then calculated based on Mie theory of light scattering. Volume distributions of the cells or cell clusters were recorded in this study and volume mean diameters were reported. Both ζ-potential and particle size measurements were taken in triplicates for each cell/cluster type.

2.7. Cell-laden alginate film preparation

To further increase the structural complexity of the engineered cell-based microstructures, native yeast cells or the cell clusters were embedded in an alginate film. The alginate film with enclosed cells or cell clusters was prepared as follows: 0.53 g of NaAlg was added to 20 mL of ultrapure water while agitating at 400 rpm to ensure complete hydration of NaAlg powder. Then, the agitation speed was lowered to 300 rpm and the mixture was stirred at 100°C for 1 hour to ensure complete dissolution of the alginate in water. Afterwards, the alginate solution was cooled to room temperature while stirred at 100 rpm. 0.2 g of glycerol was added to the solution as plasticizer. 15 mL of the prepared alginate-glycerol mixture was added to 5 mL suspension of 600 mg native cells or cell clusters in water and gently mixed with a spatula. The final composition of the solution was 2 wt.% ALG, 0.75 wt.% glycerol, 3 wt.% native cells or cell clusters. The mixture was degassed under vacuum for 15 minutes and transferred to a casting plate with 8.5 cm diameter, left to dry on a flat surface at room temperature. Dried alginate film containing native cells/ cell clusters was peeled off from the casting plate and cut into 1 cm*1 cm pieces. The alginate film

was then externally crosslinked by immersing the film pieces in pH 3.5, 5% $CaCl_2$ solution for 5 minutes, rinsed once in water, and dried to constant weight at 37°C.

2.8. Visualizing cell clusters using confocal laser scanning microscope (CLSM)

Autofluorescence properties of curcumin enabled the fluorescent imaging of curcumin infused single cells and cell clusters. A Leica TCS SP8 STED (Leica Microsystem Inc.) with a pulsed laser tuned to 488 nm was used in confocal mode for excitation. A HyD time-gated, hybrid detector was used to collect signal from 498 - 591 nm range, corresponding to the fluorescence of curcumin. For the two types of cell clusters without alginate film, z-stack images were taken before and at 40 minutes of simulated intestinal digestion. To prepare slides for confocal microscopic imaging, a 1.5 mm-thick spacer with 6 wells was placed on a glass slide, ~100 μL of 1 mg/mL cell clusters suspended in water was aliquot to each well, a coverslip was then placed on top of the spacer. Images of cell clusters before and during simulated digestion were taken with a 20X objective at the same laser intensity. The same Leica TCS SP8 STED and same settings were used in confocal mode to visualize native cells and cell clusters enclosed in alginate films. One piece of alginate film was hydrated in water and placed on glass slide covered by a coverslip. A 63x objective was used instead. 3D projection of z-stack images was performed in Fiji[22]. Texture features extraction (Haralick features) was performed using the mahotas package[23] in Python 3.7.6.

2.9. *In vitro* simulated gastric and intestinal digestion

Simulated gastric fluid (SGF) was prepared according to the procedure described by Tikekar et al.[24] with some modification. Briefly, it consists of 3.2 mg/mL pepsin in 5 mg/mL NaCl solution at pH 3.5 (pH adjusted by HCl). pH of a fasted stomach is normally below 2[25]. However, the gastric pH would rise to above 5 after food intake[26] and returned to fasted pH after secretion of hydrochloric acid. The pH of SGF chosen in the current study was around the mean value of the

gastric pH within a 2-hour digestion period after food intake, and within the range of optimum pH for pepsin activity, as recommended by Minekus et al[27]. Before simulated gastric digestion, SGF was pre-warmed to 37°C. In 1.5 mL microcentrifuge tubes, aliquots of SGF (1 mL) were added to 10mg of curcumin loaded native cells or cell clusters; or to 1 piece of 1 cm*1 cm alginate film containing native cells or cell clusters. The microcentrifuge tubes were incubated horizontally in a rotatory incubator at 37°C and 90 rpm for 2 hours. At 0, 1, and 2 hours, one sample was removed from the incubator, centrifuged, decanted, and stored in the dark for further analysis. Cell cluster samples used in subsequent intestinal digestion were removed from the incubator after 2 hours and left static until clusters precipitated down and then supernatant was removed.

Simulated intestinal fluid (SIF) was prepared as described by Tikekar et al.[24] Briefly, a stock solution containing 0.025 M potassium dihydrogen phosphate, 3.33 mg/mL $CaCl_2$ and 5 mg/mL NaCl was prepared and adjusted to pH 7.5. The stock solution was pre-warmed to 37°C. Bile salt and lipase from porcine pancreas were added to the stock right before the digestion started. The current study used two bile salt levels: 5 mg/mL for low bile salt (LBS) condition, and 25 mg/mL for high bile salt (HBS) condition. Lipase content was kept constant at 2 mg/mL for both conditions[7]. Samples from the previous gastric digestion step were re-suspended in SIF to yield a ratio of 10 mg of cells to 1mL of SIF. The microcentrifuge tubes were incubated horizontally in a rotatory incubator at 37°C and 90 rpm for up to 3 hours. One sample was removed from the incubator at 0, 1, 2, and 3 hours of digestion. After centrifugation and decanting, samples were saved for analysis. The time 0 samples were centrifuged right after addition of SIF to study whether there was any immediate curcumin release.

All simulated digestion experiments were done in triplicates for each cell-based microstructure.

2.10. Swelling test of alginate films

The equilibrium swelling test was performed at 37°C in enzyme-free, and bile salt-free simulated gastric and intestinal fluids, prepared as specified in section 2.9. Before the swelling test, the alginate films were cut into 1 cm*1 cm square pieces and dried at elevated temperature until constant weight (w_0). Then the dried films were immersed in either SGF or SIF. The weights of swelled films (w_1) were measured at predetermined time points until reaching equilibrium. The swelling ratio will be calculated as: $swelling\ ratio(\%) = \frac{w1 - w0}{w0} \times 100$. The swelling kinetics experimental data were fitted to two empirical models, namely Peleg's model (1)[28], and exponential association equation model (2)[29]. Both models have been used to fit the swelling kinetics of polymer hydrogels[30].

$$SR(t) = \frac{t}{k_1 + k_2 t}, \qquad (1)$$

where SR(t) is the swelling ratio at time t, k_1 is the kinetic constant (min*g (d.b)/g), and k_2 is the characteristic constant of the model (g (d.b)/g).

$$SR(t) = SR_e[1 - expexp\,(-k_{R1}t)\,], \qquad (2)$$

where SR_e is the swelling ratio at equilibrium (last time point), and k_{R1} is the kinetic constant (h^{-1}).

2.11. Curcumin extraction and quantification

For quantification of curcumin encapsulation yield and retention of curcumin within cell microstructures after *in vitro* digestion, curcumin was first extracted and then quantified using a UV-Vis spectrophotometer (GENESYS 10S Series, Thermo Scientific). 1 ml of acidified methanol (1 vol.% of concentrate HCl) was used for extracting curcumin from 10 mg of native cells/ cell clusters (on a wet basis), or 1 piece of 1 cm*1 cm alginate film containing cells. Samples were then vortexed, bath sonicated for 10 minutes (Branson 2510, Branson Ultrasonics) and centrifuged at 13200 rpm for 10 minutes. 800 µL of the supernatant was pipetted into a disposable cuvette

and the absorbance at λ = 426 nm was measured. A blank was prepared from each control sample (same procedures without encapsulation of curcumin) extracted in acidified methanol. The concentration of curcumin in extractant was calculated with reference to a regression equation (linear plot with slope of 0.1326) obtained from a calibration curve of curcumin in acidified methanol. All measurements were done in triplicates. Encapsulation yield of curcumin into native yeast cells was calculated based on the following equation:

$$Encapsulation\ yield\ (\mu g/mg) = \frac{C_E(\mu g)}{C_Y(mg)}$$

where C_E is the mass of curcumin extracted from the yeast cell carriers, and C_Y is the mass of the extracted yeast cells.

Fraction of curcumin retained within the cell-based microstructures after digestion was calculated based on the following equation:

$$Fraction\ retention\ of\ curcumin = \frac{C_E(t)}{C_E(t = 0\ at\ gastric)}$$

where C_E (t) is the mass of curcumin retained in the cell-based microstructure at a given time point during simulated digestion, and C_E (t=0 at gastric) is the mass of curcumin in the microstructure at time 0 of gastric digestion phase.

2.12. Statistical analysis

Statistical analyses were performed in R version 3.4.2. One-way ANOVA was used to evaluate the change in cell surface charge after polyelectrolytes deposition, and the change in particle size after cell clustering. A two-way ANOVA model was used to study the effect of structural complexity on the release profile of curcumin from all cell-based microstructures during *in vitro* simulated digestion. A separate set of samples was prepared for each time point, therefore the

samples across time points were considered independent. At each time point during simulated gastric and intestinal digestion, fraction retention of curcumin in the cell-based microstructures was defined as a function of cell clustering, extracellular alginate film addition, and their interaction term. In addition to the initial analysis, post hoc pairwise comparisons with Tukey's adjustment were conducted to determine any significant difference between groups. Significant values ($p<0.05$) were reported. No statistical analysis was conducted across time points.

3. Results

3.1. Layer-by-layer deposition of polyelectrolytes on yeast cells and electrostatic interaction facilitated cell clustering

Successful coating of alternating cationic and anionic polyelectrolytes on yeast cells was evaluated using zeta potential measurement after each deposition step, as indicated in **Figure 1**. Native yeast cells exhibited a slightly net negative surface charge (-2.36±0.39 mV) before coating due to the presence of amino groups, carboxyl groups, and phosphoryl groups on the cell surface[31,32]. Deposition of cationic PDADMAC onto the cell surface changed the zeta potential to 20.2±1.11 mV. This change was attributed to the cationic ammonium group of PDADMAC. Secondary deposition of anionic DSS or ALG onto PDADMAC@yeast again reversed the surface charge to -4.01±0.91 mV and -3.88±0.21 mV, respectively, due to the sulfate groups in DSS and carboxylic acid groups in ALG. The particle size distribution of yeast cells after each coating step was evaluated based on light scattering measurements, and the volume mean diameters ($D_{4,3}$) were calculated (**Table 1**). There was no significant increase in the volume mean diameter of yeast cells after PDADMAC coating (6.13±0.22 μm). This lack of change in particle size was attributed to the steric hindrance and electrostatic repulsion among coated yeast cells. However, with the deposition of DSS and ALG onto PDADMAC@yeast, $D_{4,3}$ of PDADMAC/ALG@yeast and

PDADMAC/DSS@yeast increased to 19.62±0.44 μm and 52.67±2.96 μm respectively, compared to ~6 μm of native and PDADMAC@yeast cells.

After LbL polyelectrolytes coating on yeast cells, one form of cell cluster architecture was formed by mixing PDADMAC@yeast and PDADMAC/ALG@yeast at a 1 to 5 (wt. to wt.) ratio in pH 3.5, 0.5% NaCl solution. This is the same physicochemical condition as in the simulated gastric fluid. This specific condition was selected for forming cell clusters to ensure that the cell clusters would not dissociate during the simulated gastric digestion. When mixed at the selected ratio, instantaneous cell aggregation was observed, resulting in cell clusters (**P+P/A cluster**) with a volume mean diameter of 62.28±1.12 μm (**Table 1**). In the case of DSS coated PDADMAC@yeast, aggregation of cells was observed upon deposition of DSS coating. Thus, these cell clusters were directly used as the second cell cluster architecture, referred to as the **P/D cluster**, for subsequent characterization. As shown in **Figure S1**, native cells and cell clusters all showed unimodal distribution, while native cells have a narrower peak than both cell clusters. **Figure 2** shows the 3D visualization of the two cell cluster architectures with encapsulated curcumin. The cell clusters constructed were in irregular shapes and loosely bound structures. The size of the cell clusters in the microscopic images was in the same size range as those measured using the particle size analyzer.

3.2. Cell clusters during *in vitro* digestion: structural stability and release of curcumin

3.2.1. Structural stability of cell clusters

Before investigating the release profile of encapsulated curcumin during simulated digestion, the structural stability of cell clusters in the simulated digestion fluids was evaluated. Since both the selected cell clusters, P+P/A cluster, and P/D cluster, were formed under the same set of pH and salt concentration as the SGF buffer, no significant

change in the particle size of the cell clusters was observed after 2 hours of simulated SGF treatment (data not shown). During simulated intestinal digestion (**Table 1**), P/D clusters retained the original size of around 50 μm after the 3 hours incubation with SIF, low or high bile salt content. For the P+P/A clusters, a significant decrease in the particle size was observed after intestinal digestion. The volume mean diameter of P+P/A clusters decreased from 62.28±1.12 μm to 48.25 μm in the presence of low bile salt SIF, and to 45.45 μm in the presence of high bile salt SIF. The change in particle size distribution after SIF treatment is shown in **Figure S1**. For the P+P/A cluster, no new peaks or significant change in the width of peaks was observed even with a reduction in the peak value after simulated digestion. In addition, the size change was observed immediately after the cell clusters were transferred to the SIF medium, while no further changes in the particle size of cell clusters were observed with extended incubation with SIF conditions.

3.2.2. In vitro release of encapsulated curcumin

Retention of curcumin during the 2-hour simulated gastric digestion was expressed as the fraction of curcumin retained in cell-based microstructures at each time point during gastric digestion as compared to their original curcumin content. As shown in **Figure 3**, all cell microstructures evaluated in this study retained ~80~95% of the initial curcumin content at the end of the 2-hour gastric phase, and no significant difference was observed between single cells and cell clusters. This result suggested that the native yeast itself as a carrier was sufficient to maintain its structural integrity and ensure the stability of curcumin under the current simulated gastric condition. Therefore, the effect of additional structural complexity on curcumin retention could not be observed during the simulated gastric digestion.

All samples were then subjected to a subsequent simulated intestinal digestion, where the release profile of curcumin in two SIF formulas with different bile salt levels was evaluated: 5 mg/mL (low bile salt) and 25 mg/mL (high bile salt). These SIF compositions with different levels of bile salt were selected based on the results of a prior study that illustrated the influence of bile salt concentration on the release rate of curcumin from yeast cells[17]. As shown in **Figure 4a,** immediately upon adding low bile salt SIF, curcumin retention decreased from ~90% after gastric digestion to 48±2% and 54±5%, respectively, in both single yeast cells and P+P/A clusters without alginate film. P/D cluster was an exception in which 79±9% of curcumin was still retained. The initial release of curcumin from cell carriers and their clusters was more significant for the high bile salt SIF condition (**Figure 4b**), where only 22±1%, 46±13%, and 26±5% of curcumin was retained at time 0 in SIF, for single cells, P/D clusters, and P+P/A clusters respectively. P/D clusters had a significantly higher resistance to the initial release of curcumin than single cells and P+P/A clusters under both bile salt levels. Under low bile salt conditions, such resistance persisted for 1 hour (**Figure 4a**), whereas for high bile salt conditions, the P/D clusters only showed significantly stronger resistance to curcumin release than the other two cell microstructures at t=0 (**Figure 4b**). The release profile of P+P/A clusters was not significantly different from that of native yeast cells throughout the intestinal digestion period for both bile salt conditions. It was also observed that P/D clusters are more stable than P+P/A clusters during simulated intestinal digestion, indicated by an immediate reduction in particle size in P+P/A clusters upon addition of SIF, as shown in **Table 1**. Such a difference might be attributed to the different ways the cells were assembled in the two types of cell clusters, which could impact the curcumin release profiles. To visualize the curcumin release

process during simulated intestinal digestion, P/D clusters and P+P/A clusters were sampled 1 minute and 40 minutes after the addition of SIF. The samples were imaged using confocal fluorescence microscopy. **Figure 5** illustrated the representative cross-section images of the two types of cell clusters during simulated intestinal digestion. The fluorescence intensity in the microscopic images showed a trend consistent with the curcumin release data: cell clusters in high bile salt SIF retained less curcumin after 40 minutes, and especially under low bile salt SIF conditions, the P/D clusters retained more curcumin than P+P/A clusters up to 40 minutes. Moreover, the decay of curcumin fluorescence overtime did not depend on the spatial localization of cell carriers within the cluster; rather, homogeneous reduction in fluorescence intensity throughout the cluster cross-section was observed. It implied that at least after 40 minutes in SIF, there was no difference in the release of curcumin from cells at different locations within the constructed cell clusters.

3.3. Cell-laden alginate films during *in vitro* digestion: structural stability and release of curcumin

3.3.1. Alginate film structural stability

To achieve a higher level of structural complexity, single cells or cell clusters containing curcumin were further encapsulated in a calcium-crosslinked alginate film. The cells or cell clusters accounted for approximately half of the dry mass of the prepared films. The loading of cells/ cell clusters in alginate film was about 2.8 mg (d.b.)/cm^2. The prepared alginate films containing native yeast cells and the two types of cell clusters were observed under a confocal microscope to confirm the integrity of the cell cluster structures in alginate film. The 3D projection of all three types of alginate films is shown in **Figure**

6. Alginate films with cell clusters could be easily differentiated from those with native cells despite the high cell density. Native cells were uniformly distributed in the alginate film, whereas the cell clusters showed obvious aggregation and voids. Haralick features were extracted from individual slices of the z-stack image compiles (**Figure S2**) to describe the image texture properties. **Table S1** tabulates three texture features: angular second moment (ASM), contrast, and correlation. Images of alginate films with native cells, P/D clusters, and P+P/A clusters had, in this order, increasing ASM, decreasing contrast, and increasing correlation. As shown in **Figure S2**, the images of cell clusters showed larger areas of background signal than that of native cells, resulting in a larger ASM value. Higher ASM values indicate a higher degree of homogeneity in the image intensity within an image. Lower contrast and higher correlation in cell cluster images translate to less local variation and a higher degree of spatial correlation of signal intensity between adjacent pixel points. All the texture features concurred with the observation from the images.

Regarding the integrity of alginate films during the simulated digestion, the film thickness was measured before and after digestion (**Table 2**). There was no significant difference in the film thickness among alginate films containing the three different cellular structures (native vs. P/D cluster vs. P+P/A cluster). Expansion of films and a slight increase in the film thickness were observed after 5 min of initial hydration of the films in water due to swelling. After the 5-hour sequential digestion, the films remained intact, and only a slight decrease in the film thickness was recorded after intestinal digestion.

To account for the effect of pH on the water absorption behavior of the films, the films were characterized for their swelling behavior in an enzyme-free SGF and an enzyme/ bile salt-free SIF. Enzymes and bile salt were excluded to eliminate the effect of potential

interactions of these biochemicals with the polymeric gel and its influence on gravimetric measurements. The swelling kinetics of alginate films with individual cells and cell clusters in SGF and SIF and the model fitting results are shown in **Figure S3** and **Table S2.** Alginate films swelled faster and to a greater extent in enzyme-free and bile-salt-free SIF than SGF. There was no substantial difference in swelling behavior among the films embedded with different cell structures, including individual cells and cell clusters.

3.3.2. In vitro release of curcumin from single cells and cell clusters within ALG films

All cell microstructures, with or without the alginate film, could retain over 80% of the encapsulated curcumin in yeast during simulated gastric digestion (**Figure 3**). However, upon the addition of SIF, only cell microstructures within alginate film were able to resist the initial release of encapsulated curcumin. Immediately after adding SIF, a significant amount of encapsulated curcumin was released from all cell microstructures without alginate film (~ 30% released under the low bile salt condition, ~ 50% under high bile salt), except for the P/D clusters (**Figure 4**). The barrier effect of alginate film to curcumin release persisted throughout the 3-hour simulated intestinal digestion under both bile salt level conditions. Under the low bile salt condition, the release profile of curcumin from single cells and P+P/A clusters were similar, where the fraction of curcumin retained in samples with alginate film was about 20-30% higher than those without alginate film for up to 2 hours. At t = 3 hours in the low bile salt condition, no significant difference was detected with and without extracellular alginate films. As shown in **Figure 4a**, the release response of curcumin from the P/D cluster with and without film was not significantly different during the first hour of incubation with low bile salt SIF. The only significant difference in curcumin retention between these two groups with and without alginate films

was observed after 2 hours. In **Figure 4b**, under the high bile salt condition, samples with alginate film had significantly higher curcumin retention than those without alginate film at all time points for all cell microstructures. For single cells and cell clusters, the most substantial release of curcumin occured during the first hour of intestinal digestion. After the first hour, all three cell microstructures without alginate film retained less than 10% of curcumin. This number further decreased down to below 5% at the end of the 3-hour intestinal digestion period. With the barrier effect of alginate film, the final curcumin retained in single cells, P/D cluster, and P+P/A cluster was at the level of 14±3%, 28±5%, and 22±4%, respectively.

Table S3 summarized the ANOVA model for curcumin retention associated with the two key variables: cell clustering and ECM (alginate film). There was a significant interaction effect between these two factors for all the time points in high bile salt SIF and the first hour for the low bile salt SIF. The interacting effect illustrates the impact of cell clustering on curcumin retention was dependent on the presence of the extracellular alginate film, as shown in **Figure 4**. In high bile salt SIF (**Figure 4b**), a significant effect of cell clustering on curcumin retention was only observed when the cell microstructures were encapsulated in alginate films. In low bile salt SIF, when no alginate film was present, P/D clusters showed higher curcumin retention in the first hour, but after the introduction of the film, the retention of curcumin in cells and P+P/A clusters was increased to the same level as P/D clusters (**Figure 4a**).

4. Discussion

4.1. LbL deposition of polyelectrolytes on the cell surface and cell clustering

Electrostatic aggregation of colloidal particles and cells has been used to create micro scale assemblies with unique properties[20,33–36]. For example, controlled electrostatic assembly of metal nanoparticles was used for generating capsules and films for material science and nanomedicine applications[36]. To the best of our knowledge, micron-scale, cell-based bioactive delivery systems formed by electrostatic clustering have not been evaluated for their performance during simulated digestion. The current study used layer-by-layer deposition of oppositely charged polyelectrolytes to assemble yeast cells to form cell clusters. PDADMAC@yeast and native yeast cells had a similar particle size distribution, but deposition of negatively charged ALG and DSS onto PDADMAC@yeast increased the particle size of the yeast cells to a different extent, although they had similar net surface charge. Similar droplet aggregation was reported in previous studies where medium molecular weight chitosan (Mw 190 -310 kDa) were deposited onto the negatively charged interface of primary emulsion[37,38]. The difference in clustering behavior of yeast cells with the addition of an anionic coating layer can be attributed to the following factors: (1) Compared with ALG, DSS has a higher charge density (charge per unit), and thus more strongly associated with PDADMAC. According to the product specification provided by the manufacturer, DSS used in the current study had approximately 2.3 sulfate groups per glucosyl unit. ALG, based on its chemical structure, had one carboxyl group per monosaccharide unit. (2) With a smaller molecular weight, DSS was added at a higher molar concentration than ALG, which may result in more clustering among PDADMAC@yeast cells. (3) The positively charged quaternary ammonium group in PDADMAC has a stronger interaction with the sulfate groups in DSS than with the carboxyl groups in ALG[39]. As a result of the different clustering behavior of DSS and ALG, two different types of cell clusters were generated. P/D clusters were harvested directly after adding DSS to PDADMAC@yeast, while P+P/A clusters were formed by mixing a positively charged

PDADMAC@yeast and a negatively charged PDADMAC/ALG@yeast at a ratio of 1:5, which resulted in the largest cell clusters. Due to the different preparation steps, P/D clusters and P+P/A clusters essentially differ in their aggregation mechanisms. P/D clusters were held together by DSS acting as crosslinkers among large PDADMAC polymers that coated yeast cells. In contrast, P+P/A clusters were formed by electrostatic attraction between oppositely charged cells. Such different clustering mechanisms translated to significantly different cluster sizes (**Table 1**) and potentially different cellular arrangements within a cluster.

4.2. Structural stability of cell clusters and cell-laden alginate films during simulated digestion

A significant size reduction in cell clusters was observed during intestinal digestion for the P+P/A cluster but not for the P/D cluster. It was hypothesized that the change in pH and salt content in the fluid caused the change in cluster size. Given that the pH of SIF (7.5) is higher than pKa of both DSS and ALG, and the quaternary ammonium cation in PADMAC is independent of pH, the surface charges of all cell types should hold during this pH transition. The high salt content in SIF, on the other hand, would have a significant impact on the effective surface charge of the oppositely charged cells. Especially the divalent calcium ions in SIF will have a more substantial charge screening effect on charged yeast cells, leading to mitigated electrostatic interactions. As discussed earlier, DSS could have a more robust interaction with PDADMAC and it was present at a higher molar concentration. Thus, the DSS facilitated crosslinking in P/D clusters could be potentially less affected by the screening effect, accounting for the higher stability of P/D clusters than P+P/A clusters.

The cell-laden alginate films were overall stable after 5 hours of simulated digestion without significant mass loss or fragmentation. In our preliminary experiments, alginate films without

calcium crosslinking would dissolve after 30 minutes of incubation in water. Thus, the presence of calcium ions in the alginate film was critical for maintaining the film integrity throughout the simulated digestion. A slight decrease in the film thickness was observed after 3 hours of simulated intestinal digestion. This decrease could be explained by the gradual release of calcium ions from crosslinked alginate film in the presence of bile salt in the intestinal fluid. Bile could bind with the calcium ions diffuse out from the alginate films and form a white precipitate, which was observed during intestinal digestion, especially with high bile salt levels. No bile salts were present in the gastric phase. Thus, neither white precipitate nor decrease of film thickness was observed after the gastric digestion. Losing calcium made the alginate network less rigid, and the film could start dissolving into the water from the surface, corresponding to the decrease in film thickness. Regardless, the alginate films could still retain their shape and integrity throughout the 3-hour intestinal digestion period.

4.3. *In vitro* release of curcumin from different cell-based structures during simulated digestion

Bioaccessibility of curcumin is significantly limited by its poor solubility, and various encapsulation methods have been developed to address this limitation, mostly using nanoparticles[40,41] or nano-emulsions[42]. Different factors such as droplet size, type of oil/emulsifier, etc., could all affect the stability and bioaccessibility of curcumin in such encapsulation systems, which has been reviewed elsewhere[43]. However, to the authors' best knowledge, there are no prior studies about the effect of food matrix microstructures on curcumin bioaccessibility, except one that reported increased curcumin accessibility during simulated digestion in the presence of excipient emulsions, which mimicked a simplified food matrix effect[44]. This previous study essentially was still addressing the solubility issue of curcumin without further considering the role

of food microstructures in controlling the release of curcumin. Among the very few studies that focus on the relationship between the structural complexity of plant tissues and the release of phytochemicals during digestion, Palmero et al.[45] evaluated the effect of natural structural barriers on carotenoids bioaccessibility in carrots. In this previous study, carrot tissues were broken down into fractions with different levels of structural complexity, from cell clusters to chromoplast, then to carotenoid enriched oil. An increase in bioaccessibility was observed with removing structural barriers in the carrot tissues[25]. Although this previous study also considered the effect of structural complexity on bioactive release, with a top-down approach, it is impossible to decouple the effects of physical cell aggregation from the extracellular matrix. To the best of our knowledge, the current study is the first one that used a bottom-up approach to investigate the relationship between structural complexity and bioactive bioaccessibility in cell-based structures.

Approximately10% of curcumin release was observed after 2 hours of *in vitro* gastric digestion (**Figure 3**). This result agrees with the limited literature data about curcumin release from yeast cells[17,46]. Since no obvious rupture of cell wall and membrane or cell burst was observed after *in vitro* gastric digestion according to microscopic images[17], the release of curcumin during digestion was attributed to passive partitioning of curcumin from cells to the digestion fluid. With a log P value of 3.29, curcumin is a hydrophobic compound with very low water solubility (0.6 μg/mL)[47]. In the absence of emulsifiers or surfactants such as bile salts, limited release of curcumin in the gastric environment was observed[46]. These results also suggest that the guest-host interaction of curcumin with cellular components of yeast cells has high avidity resulting in a limited release of curcumin[2].

Cell bases carriers after gastric digestion were treated with simulated intestinal fluid to simulate the gastrointestinal digestion process. Upon the addition of SIF, immediate release of curcumin

from single yeast cells was observed. The extent of release of curcumin from these cells was a function of the bile salt level in the fluid (**Figure 4**). Bile salts are physiological surfactants that enhance fat digestion and the absorption of hydrophobic compounds[48]. Due to their amphiphilic nature, bile salts can self-associate to form micelles in water, and the presence of these micelles in the aqueous phase can influence the partitioning properties of curcumin between yeast microcarriers and the aqueous phase. Therefore, the SIF was likely to have a higher solubilizing capacity of curcumin. Less than 30% and 5% of curcumin were retained inside single yeast cells at the end of the 3-hour intestinal digestion under low and high bile salt conditions, respectively. This trend supports the hypothesis that bile salt micelles in the SIF can shift the partitioning equilibrium of curcumin between yeast cells and the aqueous phase. Another possible explanation for the observed release of curcumin during SIF treatment is the change in cellular composition, such as changes in cell membrane composition due to the extraction of phospholipids by bile salts. These changes may influence the binding interaction between curcumin and cellular structures.

Based on the results shown in **Figure 4**, during *in vitro* digestion, the cell clustering effect on impeding the release of curcumin was limited to the early stage of intestinal digestion. The most significant difference between single cells and cell clusters was within the first hour of SIF incubation (low bile salt) or at the stage of the initial release of curcumin immediately after adding the SIF (high bile salt). Despite the formation of cell clusters by electrostatic interaction, after this initial stage, the release of curcumin during simulated intestinal digestion was not only limited to the outer cells in the clusters but rather a uniform release throughout the cluster. This is supported by the homogeneous reduction in fluorescence intensity of curcumin across the cell cluster during digestion (**Figure 5**). These results suggest that the electrostatic clustering of cells in the size range of 50 microns could not necessarily limit the interaction of bile salts in SIF with the cells in the

cluster for an extended time. This trend contrasts with the results reported in previous studies. It was shown that for cut almond seed cubes, digestion of intracellular nutrients first happened in the surface cells with the ruptured cell walls, and gradually extended to the inner intact cells over a period of 12 hours[49]. Palmero et al.[45] also reported that the bioaccessibility of β-carotene in orange carrots was lower in large cell clusters (800~2000 μm) than in small cell clusters (40~250 μm). However, unlike the plant tissue fragments, the cell clusters constructed in the current study would not be considered as rigid matrices, based on their way of assembly, irregular shape, and porous structure. Also, they were much smaller in size than those reported by Palmero et al.[45] Moreover, the cell clusters in the previous studies were a result of breaking down wholesome plant tissues, thus including the combined effect of cell clustering and associated extracellular matrix.

Upon the addition of the crosslinked extracellular alginate film, the cell microstructure matrices became less porous and more rigid. The hydrated alginate film enclosing single cells or cell clusters was a highly crosslinked hydrogel that could limit permeation of acid, enzymes, and bile salts, potentially converting the curcumin release from the "bulk erosion" mode to the "surface erosion" mode[50]. The diffusion coefficient of protons in polysaccharide hydrogels is not expected to differ from that in water[51]. However, the depletion of protons due to protonation of D-mannuronate and L-guluronate residues of alginate could still limit acid permeation into the hydrogel. Such a hypothesis is supported by the observations reported in several probiotics *in vitro* survival studies that polysaccharide gels such as alginate significantly increased the survival rate of probiotics in an acidic environment[52,53]. The same studies also showed that polysaccharide hydrogels significantly increased the survival rate of probiotics exposed to bile salt solutions. Bile salt depletion was hypothetically attributed to the binding of bile salt to alginate polymers[54] and precipitation at the presence of calcium ions[55], which were gradually released from the crosslinked

alginate films during digestion. Future research is needed to investigate the contribution of these two factors to the bile salt availability throughout the digestion process. Moreover, the mutual diffusion coefficients of enzymes in polysaccharide hydrogels were around 0.2 ~ 0.4 of their self-diffusion coefficients in solution[56]. All these factors contributed to the barrier effect of the alginate film in slowing down the release of curcumin during simulated digestion.

5. Conclusion

In this work, cell-based, tissue-like microstructures were constructed using a novel bottom-up approach to study the effect of cell clustering and the role of extracellular matrix on bioaccessibility of a model bioactive compound – curcumin during *in vitro* digestion. Less than 20% of curcumin was released during gastric phase for all cell-based microstructures and the major difference in their release profiles was observed during the intestinal phase. P/D clusters, formed by crosslinking PDADMAC-coated yeast cells with DSS, had higher physical stability throughout the simulated gastrointestinal digestion process, and showed significant increase in curcumin retention at the onset of the intestinal digestion phase. Such resistance to release persisted for up to one hour in SIF with low bile salt concentration but disappeared immediately under high bile salt condition. Cell clustering also did not result in any spatial difference in curcumin release, as indicated in the fluorescence microscopic images. Addition of extracellular alginate film to both single cells and cell clusters further slowed down the release of curcumin. The retention of curcumin in cell microstructures with the alginate film was significantly higher than the corresponding cell microstructures without the film for up to 2 hours under low bile salt condition and up to 3 hours under high bile salt condition. In summary, the extracellular alginate film had a more dominating and prolonged effect on modifying the release profile of encapsulated curcumin

during simulated digestion compared to cell clustering. The bottom-up approach used in this work successfully decouples the effect of chemical composition and microstructural properties of food matrices on bioaccessibility of micronutrients. It is a versatile approach that can provide insights into the structure-bioaccessibility relationship between various micronutrients and natural or functional foods.

Author contributions

Yixing Lu: conceptualization, investigation, formal analysis, methodology, writing - original draft, writing – review & editing

Rewa Rai: conceptualization, funding acquisition, writing – review & editing, supervision

Nitin Nitin: conceptualization, funding acquisition, writing – review & editing, supervision

Conflict of interest

There are no conflicts of interest to declare.

Acknowledgement

This work was funded by a grant from the USDA-NIFA grant no. 2018-67017-27563. The fluorescence microscopic images were taken at the UC Davis Veterinary Medicine Advanced Imaging Facility.

Tables

Table 1: Particle size of cell microstructures before and after *in vitro* intestinal digestion. *

	Particle size of different cells structures (μm)		
	Native yeast	P/D cluster	P+P/A cluster
Before digestion	5.77±0.14 ^{Aa}	52.67±2.96 ^{Ba}	62.28±1.12 ^{Ca}
After low bile salt digestion	5.57±0.22 ^{Aa}	51.95±0.88 ^{Ba}	48.25±6.06 ^{Cb}
After high bile salt digestion	5.50±0.35 ^{Aa}	52.57±1.92 ^{Ba}	45.45±1.67 ^{Cb}

* Data are shown as mean±SD of triplicate experiments. Means in the same row with different superscript uppercase letters are significantly different; means in the same column with different superscript lowercase letters are significantly different.

Table 2: Change in thickness of extracellular alginate films encapsulating cells or cell clusters during *in vitro* digestion. *

	Native yeast	P/D cluster	P+P/A cluster
Dry crosslinked [a]	0.07±0.01	0.08±0.01	0.09±0.01
Hydrated [bc]	0.11±0.01	0.11±0.02	0.11±0.01
After gastric digestion [c]	0.13±0.01	0.13±0.01	0.12±0.01
After high bile salt intestinal digestion [ab]	0.11±0.02	0.10±0.01	0.09±0.01

* Data are shown as mean±SD of triplicate experiments. Two-way mixed model ANOVA results showed that there was no significant main effect of cell structures, therefore a paired t-test was done for ALG film thickness at different stages of digestion (mean of each row), disregarding the containing cell structures. Different superscript lowercase letters indicate significant difference among row means.

Figure captions (figures submitted separately as individual files)

Fig. 1: Zeta potential of yeast cells at different steps of layer-by-layer deposition of polyelectrolytes and cluster assembly. 1mg/ml cells/clusters suspension in pH 3.5, 0.5% NaCl solution were used for the measurements.

Fig. 2: 3D projection of confocal microscope image of yeast cell clusters. Left: P/D cluster; right: P+P/A cluster. A pulsed laser tuned to 488 nm was used for excitation and emission signals were detected in the range of 498-591 nm. The images were taken using a 20X objective and the scale bar corresponds to 20 μm.

Fig. 3: Effect of cluster and alginate film on the retention of curcumin after 1h and 2h simulated gastric digestion. **"**With/ without film" stands for the presence or absence of extracellular alginate film. Different letters in columns within the same time point indicate a significant difference in retention of curcumin among different cellular microstructures. No statistical analysis was done on measurements across time points.

Fig. 4: Effect of cluster and alginate film on the retention of curcumin during post-gastric simulated intestinal digestion: (a) low bile salt condition; (b) high bile salt condition. **"**With/ without film" stands for the presence or absence of extracellular alginate film. Different letters in columns within the same time point indicate a significant difference in retention of curcumin among different cellular microstructures. "SIF t=0" samples were measured after addition and immediate removal of SIF. No statistical analysis was done on measurements across time points.

Fig. 5: Cross section fluorescence microscope images of cell clusters during simulated intestinal digestion under low and high bile salt conditions: (a) P/D cluster; (b) P+P/A cluster. The images were taken at t=0 and 40min. For t=0 images, SIF was added to cell clusters and immediately removed by centrifugation. The scale bar is 15μm.

Fig. 6: 3D projection of confocal microscope images of native cell (left), P/D cluster (middle), and P+P/A cluster (right) in alginate film. A pulsed laser tuned to 488 nm was used for excitation and emission signals were detected in the range of 498-591 nm. The images were taken using a 20X objective and the scale bar corresponds to 10 μm.

Bibliography

1. A. Shehzad, F. Wahid and Y. S. Lee, Curcumin in cancer chemoprevention: molecular targets, pharmacokinetics, bioavailability, and clinical trials., *Arch. Pharm. (Weinheim)*, 2010, **343**, 489–499.
2. M. S. Mathew, K. Vinod, P. S. Jayaram, R. S. Jayasree and K. Joseph, Improved Bioavailability of Curcumin in Gliadin-Protected Gold Quantum Cluster for Targeted Delivery., *ACS Omega*, 2019, **4**, 14169–14178.
3. K. H. van het Hof, I. A. Brouwer, C. E. West, E. Haddeman, R. P. Steegers-Theunissen, M. van Dusseldorp, J. A. Weststrate, T. K. Eskes and J. G. Hautvast, Bioavailability of lutein from vegetables is 5 times higher than that of beta-carotene., *Am. J. Clin. Nutr.*, 1999, **70**, 261–268.
4. J. R. Zhou, E. T. Gugger and J. W. Erdman, The crystalline form of carotenes and the food matrix in carrot root decrease the relative bioavailability of beta- and alpha-carotene in the ferret model., *J Am Coll Nutr*, 1996, **15**, 84–91.
5. A. Scalbert and G. Williamson, Dietary intake and bioavailability of polyphenols., *J. Nutr.*, 2000, **130**, 2073S–85S.
6. J. Boyer and R. H. Liu, Apple phytochemicals and their health benefits., *Nutr J*, 2004, **3**, 5.
7. A. Wright, C. Pietrangelo and A. Macnaughton, Influence of simulated upper intestinal parameters on the efficiency of beta carotene micellarisation using an in vitro model of digestion, *Food Chem.*, 2007.
8. P. C. Hollman, J. M. van Trijp, M. N. Buysman, M. S. van der Gaag, M. J. Mengelers, J. H. de Vries and M. B. Katan, Relative bioavailability of the antioxidant flavonoid quercetin from various foods in man., *FEBS Lett.*, 1997, **418**, 152–156.
9. K. H. van het Hof, B. C. de Boer, L. B. Tijburg, B. R. Lucius, I. Zijp, C. E. West, J. G. Hautvast and J. A. Weststrate, Carotenoid bioavailability in humans from tomatoes processed in different ways determined from the carotenoid response in the triglyceride-rich lipoprotein fraction of plasma after a single consumption and in plasma after four days of consumption., *J. Nutr.*, 2000, **130**, 1189–1196.
10. A. J. Edwards, C. H. Nguyen, C.-S. You, J. E. Swanson, C. Emenhiser and R. S. Parker, Alpha- and beta-carotene from a commercial puree are more bioavailable to humans than from boiled-mashed carrots, as determined using an extrinsic stable isotope reference method., *J. Nutr.*, 2002, **132**, 159–167.
11. M. Abid, S. Jabbar, T. Wu, M. M. Hashim, B. Hu, S. Lei and X. Zeng, Sonication enhances polyphenolic compounds, sugars, carotenoids and mineral elements of apple juice., *Ultrason Sonochem*, 2014, **21**, 93–97.
12. G. Nelson, S. C. Duckham and M. E. D. Crothers, in *Polymeric drug delivery I: particulate drug carriers*, ed. S. Svenson, American Chemical Society, Washington, DC, 2006, vol. 923, pp. 268–281.
13. E. I. Paramera, S. J. Konteles and V. T. Karathanos, Microencapsulation of curcumin in cells of Saccharomyces cerevisiae, *Food Chem.*, 2011, **125**, 892–902.
14. R. Salari, O. Rajabi, Z. Khashyarmanesh, M. Fathi Najafi and B. S. Fazly Bazzaz, Characterization of Encapsulated Berberine in Yeast Cells of Saccharomyces cerevisiae., *Iran J Pharm Res*, 2015, **14**, 1247–1256.
15. S. Young, S. Dea and N. Nitin, Vacuum facilitated infusion of bioactives into yeast

microcarriers: Evaluation of a novel encapsulation approach., *Food Res. Int.*, 2017, **100**, 100–112.
16. S. Young and N. Nitin, Thermal and oxidative stability of curcumin encapsulated in yeast microcarriers., *Food Chem.*, 2019, **275**, 1–7.
17. S. Young, R. Rai and N. Nitin, Bioaccessibility of curcumin encapsulated in yeast cells and yeast cell wall particles., *Food Chem.*, 2020, **309**, 125700.
18. Z. Zhang, R. Zhang, L. Zou, L. Chen, Y. Ahmed, W. Al Bishri, K. Balamash and D. J. McClements, Encapsulation of curcumin in polysaccharide-based hydrogel beads: Impact of bead type on lipid digestion and curcumin bioaccessibility, *Food Hydrocoll.*, 2016, **58**, 160–170.
19. B. Zeeb, A. H. Saberi, J. Weiss and D. J. McClements, Formation and characterization of filled hydrogel beads based on calcium alginate: Factors influencing nanoemulsion retention and release, *Food Hydrocoll.*, 2015, **50**, 27–36.
20. A. I. Zamaleeva, I. R. Sharipova, A. V. Porfireva, G. A. Evtugyn and R. F. Fakhrullin, Polyelectrolyte-mediated assembly of multiwalled carbon nanotubes on living yeast cells., *Langmuir*, 2010, **26**, 2671–2679.
21. A. Diaspro, D. Silvano, S. Krol, O. Cavalleri and A. Gliozzi, Single Living Cell Encapsulation in Nano-organized Polyelectrolyte Shells, *Langmuir*, 2002, **18**, 5047–5050.
22. I. I. Moraru, J. C. Schaff, B. M. Slepchenko, M. L. Blinov, F. Morgan, A. Lakshminarayana, F. Gao, Y. Li and L. M. Loew, Virtual Cell modelling and simulation software environment., *IET Syst Biol*, 2008, **2**, 352–362.
23. L. P. Coelho, Mahotas: Open source software for scriptable computer vision, *J. Open Res. Softw.*, 2013, **1**, e3.
24. R. V. Tikekar, Y. Pan and N. Nitin, Fate of curcumin encapsulated in silica nanoparticle stabilized Pickering emulsion during storage and simulated digestion, *Food Res. Int*, 2013, **51**, 370–377.
25. J. R. Malagelada, G. F. Longstreth, W. H. Summerskill and V. L. Go, Measurement of gastric functions during digestion of ordinary solid meals in man., *Gastroenterology*, 1976, **70**, 203–210.
26. L. Kalantzi, K. Goumas, V. Kalioras, B. Abrahamsson, J. B. Dressman and C. Reppas, Characterization of the human upper gastrointestinal contents under conditions simulating bioavailability/bioequivalence studies., *Pharm. Res.*, 2006, **23**, 165–176.
27. M. Minekus, M. Alminger, P. Alvito, S. Ballance, T. Bohn, C. Bourlieu, F. Carrière, R. Boutrou, M. Corredig, D. Dupont, C. Dufour, L. Egger, M. Golding, S. Karakaya, B. Kirkhus, S. Le Feunteun, U. Lesmes, A. Macierzanka, A. Mackie, S. Marze, D. J. McClements, O. Ménard, I. Recio, C. N. Santos, R. P. Singh, G. E. Vegarud, M. S. J. Wickham, W. Weitschies and A. Brodkorb, A standardised static in vitro digestion method suitable for food - an international consensus., *Food Funct*, 2014, **5**, 1113–1124.
28. M. Peleg, An empirical model for the description of moisture sorption curves, *J. Food Sci.*, 1988, **53**, 1216–1217.
29. K. G. Kaptso, Y. N. Njintang, A. E. Komnek, J. Hounhouigan, J. Scher and C. M. F. Mbofung, Physical properties and rehydration kinetics of two varieties of cowpea (Vigna unguiculata) and bambara groundnuts (Voandzeia subterranea) seeds, *J. Food Eng.*, 2008, **86**, 91–99.
30. A. S. Kipcak, O. Ismail, I. Doymaz and S. Piskin, Modeling and Investigation of the Swelling Kinetics of Acrylamide-Sodium Acrylate Hydrogel, *J. Chem.*, 2014, **2014**, 1–8.

31. M. Liu, F. Dong, W. Zhang, X. Nie, H. Wei, S. Sun, X. Zhong, Y. Liu and D. Wang, Contribution of surface functional groups and interface interaction to biosorption of strontium ions by Saccharomyces cerevisiae under culture conditions, *RSC Adv.*, 2017, **7**, 50880–50888.
32. S. M. Tazhibaeva, K. B. Musabekov, A. B. Orazymbetova and A. A. Zhubanova, Surface properties of yeast cells, *Colloid Journal*, 2003, **65**, 122–124.
33. A. Diaspro, D. Silvano, S. Krol, O. Cavalleri and A. Gliozzi, Single Living Cell Encapsulation in Nano-organized Polyelectrolyte Shells, *Langmuir*, 2002, **18**, 5047–5050.
34. S. Chien and K. M. Jan, Red cell aggregation by macromolecules: roles of surface adsorption and electrostatic repulsion., *J. Supramol. Struct.*, 1973, **1**, 385–409.
35. A. N. Shipway, M. Lahav, R. Gabai and I. Willner, Investigations into the Electrostatically Induced Aggregation of Au Nanoparticles†, *Langmuir*, 2000, **16**, 8789–8795.
36. J. P. Chapel and J. F. Berret, Versatile electrostatic assembly of nanoparticles and polyelectrolytes: Coating, clustering and layer-by-layer processes, *Curr. Opin. Colloid Interface Sci.*, 2012, **17**, 97–105.
37. S. Ogawa, E. A. Decker and D. J. McClements, Production and characterization of O/W emulsions containing cationic droplets stabilized by lecithin-chitosan membranes., *J. Agric. Food Chem.*, 2003, **51**, 2806–2812.
38. T. Aoki, E. A. Decker and D. J. McClements, Influence of environmental stresses on stability of O/W emulsions containing droplets stabilized by multilayered membranes produced by a layer-by-layer electrostatic deposition technique, *Food Hydrocoll.*, 2005, **19**, 209–220.
39. E. Dickinson, Hydrocolloids at interfaces and the influence on the properties of dispersed systems, *Food Hydrocoll.*, 2003, **17**, 25–39.
40. L. Zou, B. Zheng, R. Zhang, Z. Zhang, W. Liu, C. Liu, H. Xiao and D. J. McClements, Enhancing the bioaccessibility of hydrophobic bioactive agents using mixed colloidal dispersions: Curcumin-loaded zein nanoparticles plus digestible lipid nanoparticles, *Food Res. Int*, 2016, **81**, 74–82.
41. A. E. Krausz, B. L. Adler, V. Cabral, M. Navati, J. Doerner, R. A. Charafeddine, D. Chandra, H. Liang, L. Gunther, A. Clendaniel, S. Harper, J. M. Friedman, J. D. Nosanchuk and A. J. Friedman, Curcumin-encapsulated nanoparticles as innovative antimicrobial and wound healing agent., *Nanomedicine*, 2015, **11**, 195–206.
42. B. Zheng, S. Peng, X. Zhang and D. J. McClements, Impact of Delivery System Type on Curcumin Bioaccessibility: Comparison of Curcumin-Loaded Nanoemulsions with Commercial Curcumin Supplements., *J. Agric. Food Chem.*, 2018, **66**, 10816–10826.
43. A. Araiza-Calahorra, M. Akhtar and A. Sarkar, Recent advances in emulsion-based delivery approaches for curcumin: From encapsulation to bioaccessibility, *Trends Food Sci. Technol.*, 2018, **71**, 155–169.
44. L. Zou, W. Liu, C. Liu, H. Xiao and D. J. McClements, Utilizing food matrix effects to enhance nutraceutical bioavailability: increase of curcumin bioaccessibility using excipient emulsions., *J. Agric. Food Chem.*, 2015, **63**, 2052–2062.
45. P. Palmero, L. Lemmens, A. Ribas-Agustí, C. Sosa, K. Met, J. de Dieu Umutoni, M. Hendrickx and A. Van Loey, Novel targeted approach to better understand how natural structural barriers govern carotenoid in vitro bioaccessibility in vegetable-based systems., *Food Chem.*, 2013, **141**, 2036–2043.
46. E. I. Paramera, S. J. Konteles and V. T. Karathanos, Stability and release properties of

curcumin encapsulated in Saccharomyces cerevisiae, β-cyclodextrin and modified starch, *Food Chem.*, 2011, **125**, 913–922.
47. B. T. Kurien, A. Singh, H. Matsumoto and R. H. Scofield, Improving the solubility and pharmacological efficacy of curcumin by heat treatment., *Assay Drug Dev Technol*, 2007, **5**, 567–576.
48. N. Pavlović, S. Goločorbin-Kon, M. Đanić, B. Stanimirov, H. Al-Salami, K. Stankov and M. Mikov, Bile acids and their derivatives as potential modifiers of drug release and pharmacokinetic profiles., *Front. Pharmacol.*, 2018, **9**, 1283.
49. G. Mandalari, R. M. Faulks, G. T. Rich, V. Lo Turco, D. R. Picout, R. B. Lo Curto, G. Bisignano, P. Dugo, G. Dugo, K. W. Waldron, P. R. Ellis and M. S. J. Wickham, Release of protein, lipid, and vitamin E from almond seeds during digestion., *J. Agric. Food Chem.*, 2008, **56**, 3409–3416.
50. F. von Burkersroda, L. Schedl and A. Göpferich, Why degradable polymers undergo surface erosion or bulk erosion., *Biomaterials*, 2002, **23**, 4221–4231.
51. N. Amdursky, R. Orbach, E. Gazit and D. Huppert, Probing the inner cavities of hydrogels by proton diffusion, *J. Phys. Chem. C*, 2009, **113**, 19500–19505.
52. X. Y. Li, X. G. Chen, Z. W. Sun, H. J. Park and D.-S. Cha, Preparation of alginate/chitosan/carboxymethyl chitosan complex microcapsules and application in Lactobacillus casei ATCC 393, *Carbohydr. Polym.*, 2011, **83**, 1479–1485.
53. A. Dafe, H. Etemadi, A. Dilmaghani and G. R. Mahdavinia, Investigation of pectin/starch hydrogel as a carrier for oral delivery of probiotic bacteria., *Int. J. Biol. Macromol.*, 2017, **97**, 536–543.
54. W. Wang, M. Onnagawa, Y. Yoshie and T. Suzuki, Binding of bile salts to soluble and insoluble dietary fibers of seaweeds, *Fisheries Sci.*, 2001, **67**, 1169–1173.
55. J. J. Gu, A. F. Hofmann, H. T. Ton-Nu, C. D. Schteingart and K. J. Mysels, Solubility of calcium salts of unconjugated and conjugated natural bile acids., *J. Lipid Res.*, 1992, **33**, 635–646.
56. J. Thévenot, C. Cauty, D. Legland, D. Dupont and J. Floury, Pepsin diffusion in dairy gels depends on casein concentration and microstructure., *Food Chem.*, 2017, **223**, 54–61.

Graphical abstract

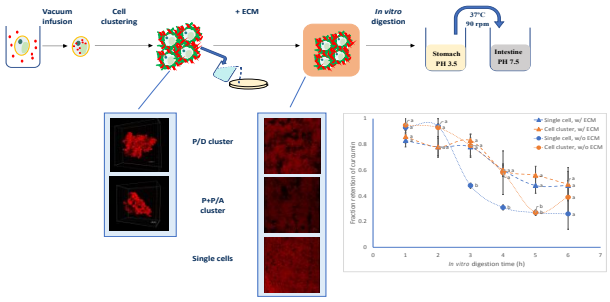

Highlight of study: This study develops a bottom-up approach to investigate the effect of food microstructures on the bioaccessibility of curcumin, enabling innovations in food structures to control the release of micronutrients.

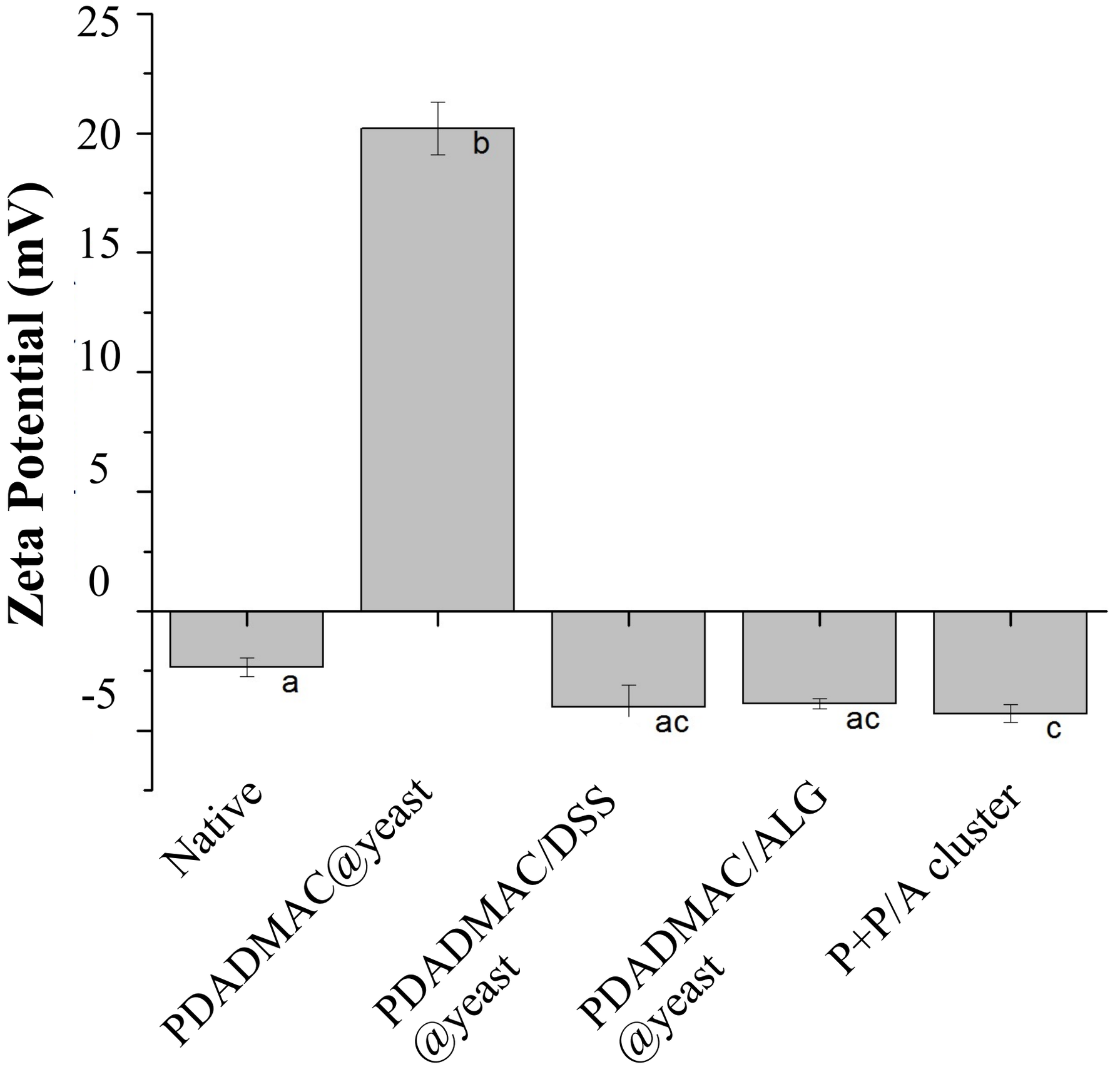
Zeta Potential (mV)
25
20
15
10
5
0
-5
a
b
ac
ac
c
Native
PDADMAC@yeast
PDADMAC/DSS @yeast
PDADMAC/ALG @yeast
P+P/A cluster

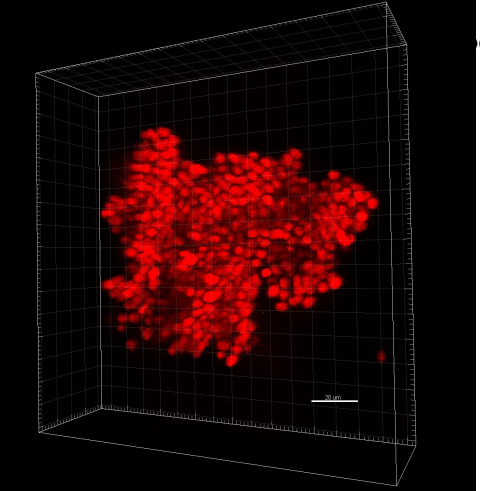
20 µm

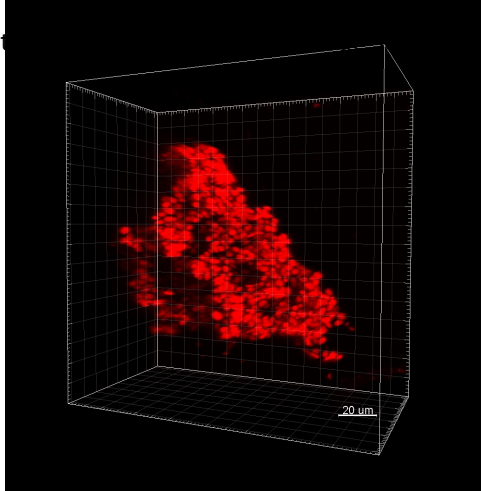
20 µm

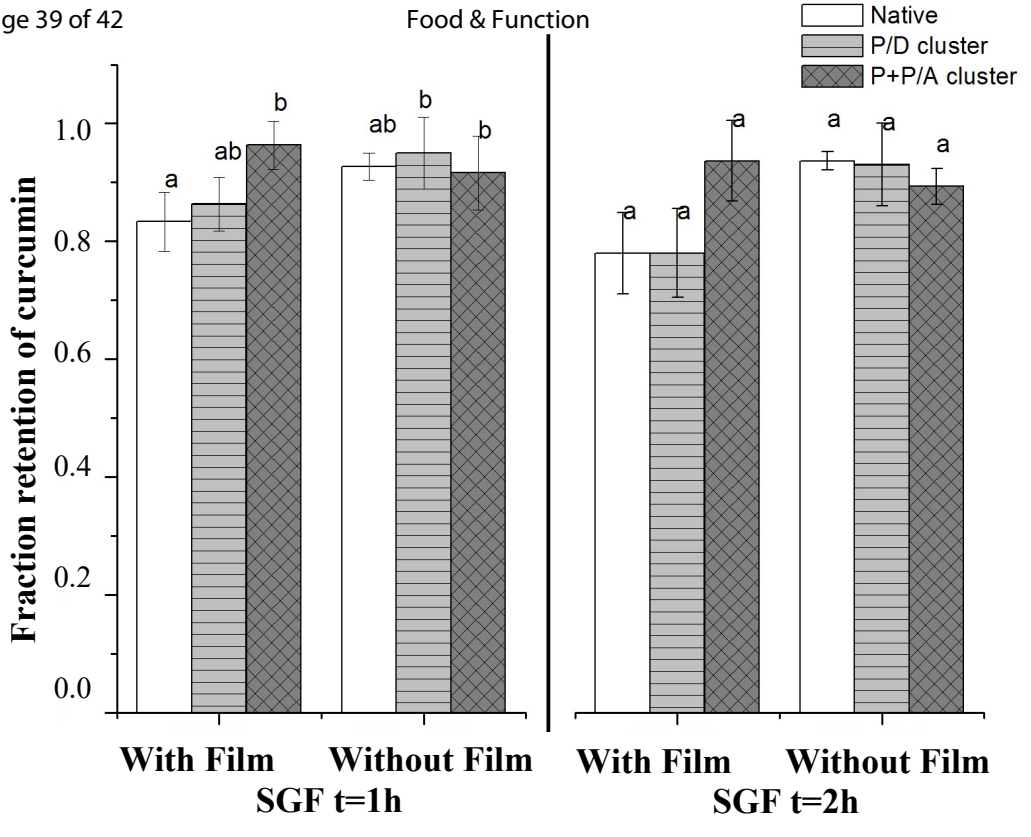
Native
P/D cluster
P+P/A cluster
Fraction retention of curcumin
0.0
0.2
0.4
0.6
0.8
1.0
a
ab
b
ab
b
b
a
a
a
a
a
a
With Film
Without Film
With Film
Without Film
SGF t=1h
SGF t=2h

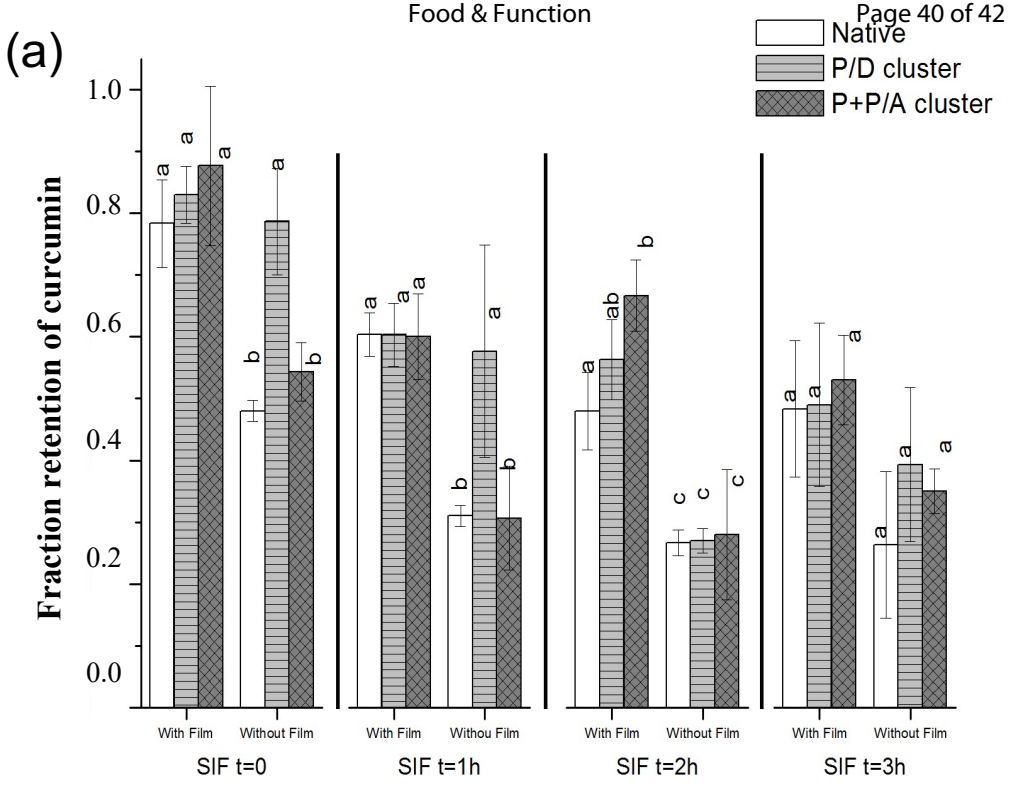
(a)
Native
P/D cluster
P+P/A cluster
Fraction retention of curcumin
1.0
0.8
0.6
0.4
0.2
0.0
With Film
Without Film
Withou Film
SIF t=0
SIF t=1h
SIF t=2h
SIF t=3h

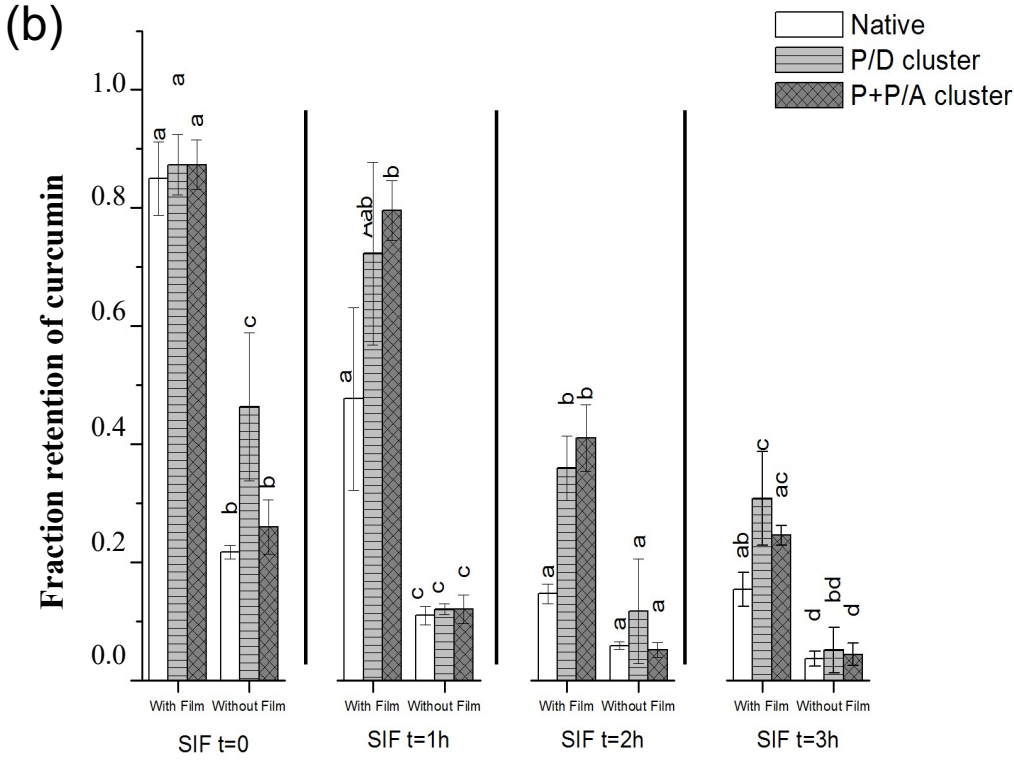
(b)
Native
P/D cluster
P+P/A cluster
Fraction retention of curcumin
1.0
0.8
0.6
0.4
0.2
0.0
With Film
Without Film
SIF t=0
SIF t=1h
SIF t=2h
SIF t=3h

(a)

Low bile salt SIF

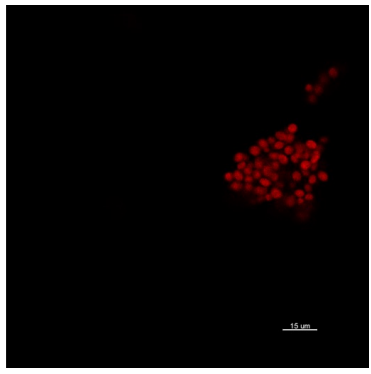

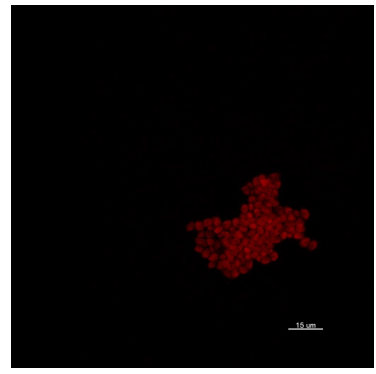

High bile salt SIF

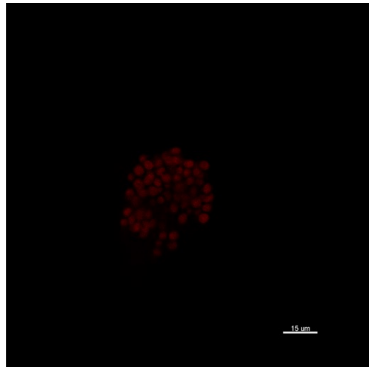

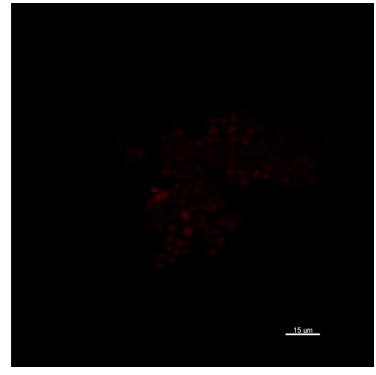

SIF t=0

SIF t=40 minutes

(b)

Low bile salt SIF

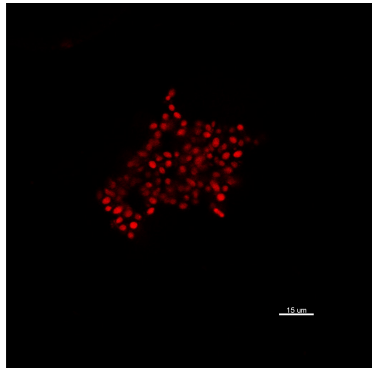

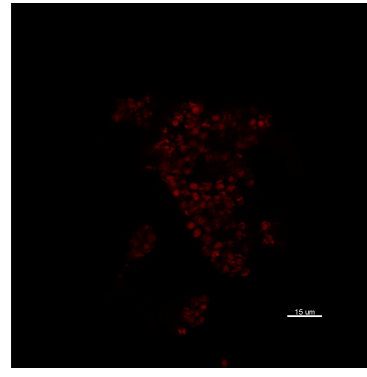

High bile salt SIF

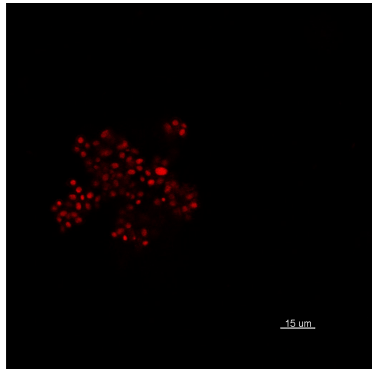

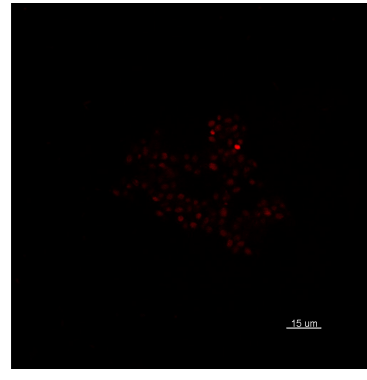

SIF t=0

SIF t=40 minutes

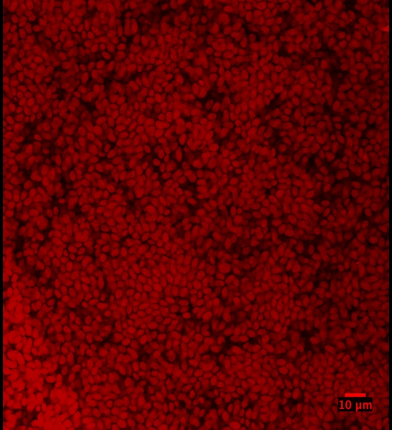
10 µm

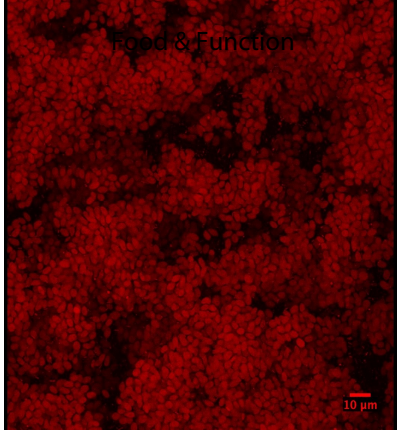
10 µm

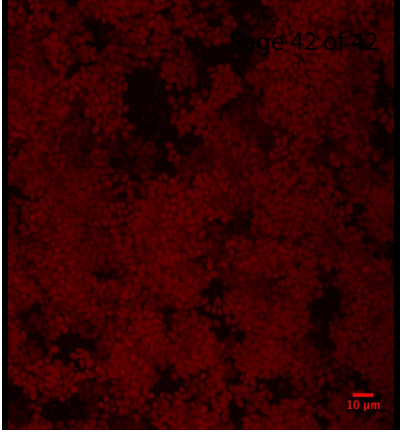
10 µm